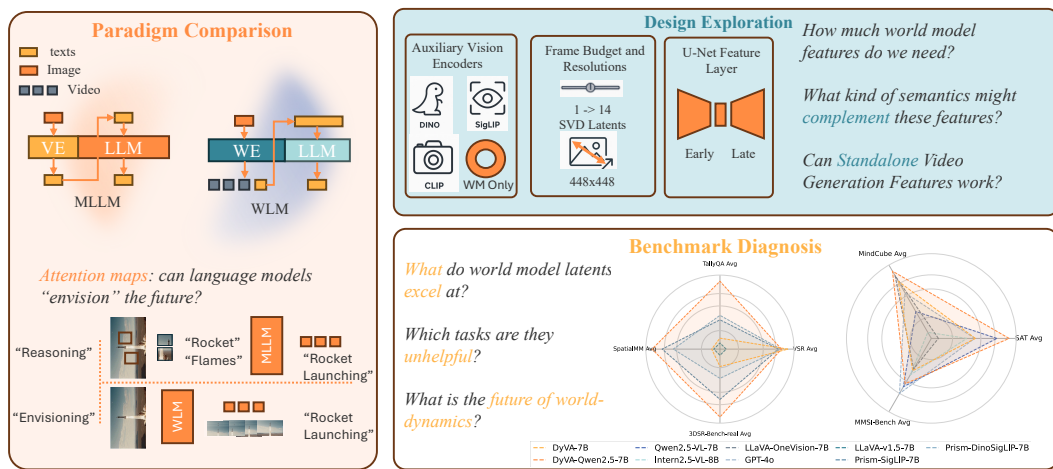


000 001 002 003 004 005 006 007 008 009 010 CAN WORLD MODELS BENEFIT VLMS FOR WORLD DYNAMICS?

005
006
Anonymous authors
Paper under double-blind review

009 010 ABSTRACT

011
012
013
014
015
016
017
018
019
020
021
022
023
024
025
026
027
028
029
Trained on internet-scale video data, world models are increasingly recognized as powerful world simulators that can generate consistent and plausible dynamics over structure, motion, and physics. While recent studies have explored the few-shot learning capabilities of world models on vision tasks, these explorations typically lack a systematic investigation of the further applicability of such methods on generic tasks. We study what happens when these priors are transferred into a Vision-Language Model (VLM): we re-purpose a video diffusion model as a *generative encoder*, queried for a single denoising step, and treat the resulting latents as an additional set of visual embeddings. We empirically investigate this class of models, which we refer to as World-Language Models (WorldLMs), and we find that generative encoders can indeed capture latents useful for downstream understanding, showing distinctions from conventional vision encoders. Naming our best-performing WorldLM **Dynamic Vision Aligner (DyVA)**, we further discover that this method significantly enhances spatial reasoning abilities and enables single-image models to perform multi-frame reasoning. Through the curation of a suite of spatial evaluation sets, we find DyVA to surpass both open-source and proprietary baselines on out-of-domain tasks, achieving **state-of-the-art performance on MindCube**. Finally, we systematically explore extensive model designs to highlight promising directions for future work. We hope our study can pave the way for a new family of VLMs that leverage priors from world models.



054 **1 INTRODUCTION**
 055

056 World models, originally proposed in cognitive science to explain how humans predict and plan in
 057 their environments (Tolman, 1948), have recently emerged as powerful tools in machine learning.
 058 Generative world models (Agarwal et al., 2025b; OpenAI, 2024; Wan et al., 2025; Hu et al., 2023;
 059 Blattmann et al., 2023; Yang et al., 2025b; Guo* et al., 2023; 2025; Chen* et al., 2025), such as
 060 video generation models (VGMs), trained on internet-scale data, encode strong priors over objects,
 061 spatial layouts, and dynamics. These priors allow them to predict plausible future scenarios that are
 062 consistent in 3D structure and physically coherent in motion

063 However, a largely overlooked implication of World Models is that the ability to generate coherent
 064 futures signals a form of semantic understanding of visual dynamics; this difference between visual
 065 generation and understanding has shaped a decade of representation learning. This suggests that
 066 world models can be more than generators—they may serve as transferable encoders that enrich
 067 downstream tasks with spatial, temporal, and predictive signals. As a result, recent works have
 068 attempted to use video generation backbones for visual perception tasks (Acuaviva et al., 2025).

069 In this work, we ask a fundamental question: *To truly understand the world, must a model first
 070 learn to predict?*

071 To empirically investigate this, we introduce a simple yet effective framework on Vision-Language
 072 Models (VLMs). We specifically explore by evaluating the applicability of predictive world models
 073 on a generic task—Visual Question Answering (VQA)—to assess their broader potential as **generalizable**
 074 **vision encoders**. Currently, mainstream VLMs primarily rely on ViT-based encoders such
 075 as CLIP (Radford et al., 2021), SigLIP (Zhai et al., 2023), and DINO (Caron et al., 2021; Oquab
 076 et al., 2024), which extract visual semantics from image patches and are then projected as visual
 077 tokens into language backbones. While these encoders are semantically aligned, they are limited
 078 by temporal reasoning and weaken spatial grounding when multiple views or sequential cues are
 079 present. On the other hand, we re-purpose a world model (Stable Video Diffusion SVD) as a novel
 080 **Generative Encoder**. Our core mechanism is to extract latent features from a **single denoising step**
 081 of its U-Net. This single step, we hypothesize, captures the low-dimensional world-dynamics prior
 082 sufficient for downstream understanding. These dynamics-aware latents are then fused with static
 083 image features (e.g., SigLIP) and projected into the LLM. The design is very efficient: all encoders
 084 remain frozen, with only lightweight projectors and the LLM being trained.

085 To this end, we conduct a systematic investigation comparatively evaluating this class of models,
 086 which we refer to as World-Language Models (WorldLMs). Our findings are as follows:

- 087 • **Shift in Reasoning Paradigm.** The generative prior alters the model’s reasoning process.
 088 It moves beyond describing static content to envisioning dynamic possibilities.
- 089 • **Zero-shot Multi-Frame Adaptation.** Trained exclusively on single images, the generative
 090 encoder enables emergent multi-frame reasoning without multi-image pre-training.
- 091 • **State-of-the-Art Zero-Shot Reasoning.** On multi-frame benchmarks, DyVA achieves
 092 state-of-the-art performance, decisively outperforming leading proprietary models such as
 093 Qwen2.5-VL (Bai et al., 2025) and GPT-4o (OpenAI et al., 2024).

095 Our best-performing WorldLM variant, **Dynamic Vision Aligner (DyVA)**, exemplifies this paradigm
 096 shift. In zero-shot evaluations on challenging multi-frame reasoning benchmarks, DyVA decisively
 097 surpasses even proprietary models, for instance, a **28.3%** lead on the **MindCube** benchmark over
 098 the GPT-4o model. This provides strong evidence that the ability to predict is a powerful, perhaps
 099 essential, foundation for stronger representation learning.

100 As shown in Figure 1, we systemically organize our investigation revolving around three pillars:

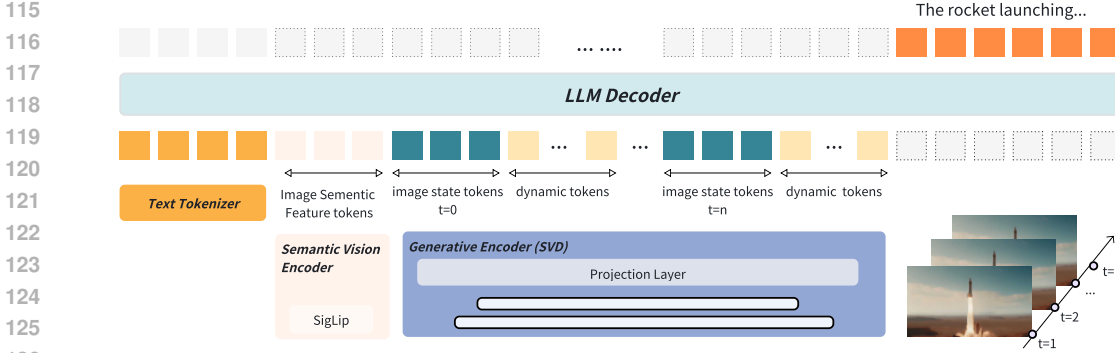
101 **Paradigm comparison.** World-model encoders versus static encoders reveal distinct strengths:
 102 world-model latents benefit spatial and multi-frame reasoning, while static encoders excel on
 103 semantics-heavy benchmarks.

105 **Benchmark diagnostics.** Through curated evaluation sets—including MindCube Yin et al. (2025),
 106 SAT-Bench Ray et al. (2024), VSR Liu et al. (2023a), we find DyVA to surpass both open-source and
 107 proprietary baselines on out-of-domain tasks, achieving **state-of-the-art performance on Mind-
 108 Cube and SATBench**. —we show that dynamics-aware latents particularly help with object rela-

108 tions, perspectives, and multi-frame spatial reasoning, while offering less gain on tasks requiring
 109 stronger language priors.
 110

111 **Design-space exploration.** We analyze different encoder setups to identify when predicted latents
 112 help or hinder performance, laying the groundwork for a new class of WorldLMs exploiting world-
 113 model priors.

114



121 Figure 2: **WorldLM Pipeline.** A SigLIP encoder extracts static semantic features from the input
 122 image. Concurrently, a Generative Encoder generates dynamic state tokens and predicts future dy-
 123 namic tokens to capture temporal changes, using evenly spaced keyframe slots. All visual tokens
 124 are projected into a shared embedding space, concatenated with text tokens, and then fed into the
 125 LLM decoder.
 126

2 PRELIMINARY

136 To ground our analysis, we need 1) a framework to incorporate the dynamic features of a world
 137 model into a multimodal language model (which we term **WorldLM**), 2) a training recipe, and 3)
 138 an implementation of inference supporting both single- and multi-image datasets.
 139

140 **Framework.** Traditional VLMs like LLaVA (Liu et al., 2024), QwenVL (Bai et al., 2025), and
 141 Prismatic-VLMs (Karamchetti et al., 2024), adopt an architecture consisting of three core compo-
 142 nents. Given an input image $x_{img} \in \mathbb{R}^{H \times W \times C}$ and a text prompt u_{prompt} , the model processes
 143 them through the following components:

- 144 • **Semantic Vision Encoder.** The input image x_{img} is processed by a frozen pre-trained ViT-
 145 based (Dosovitskiy et al., 2021) vision encoder V_ω , for example SigLIP (Zhai et al., 2023),
 146 to extract a sequence of feature embeddings $p_{img} = V_\omega(x_{img})$, where $p_{img} \in \mathbb{R}^{L \times d_{vision}}$.
 147
- 148 • **Projector.** The visual features p_{img} are subsequently mapped into the language model’s
 149 embedding space by a projector F_ψ . This yields a sequence of embeddings $e_{img} = F_\psi(p_{img})$,
 150 where $e_{img} \in \mathbb{R}^{L \times d_{text}}$. The projector is typically implemented as a simple
 151 Multi-Layer Perceptron (MLP) with GELU activations (Hendrycks & Gimpel, 2023).
 152
- 153 • **LLM Backbone.** Finally, the language model LM_θ autoregressively generates the textual
 154 output u_{out} . It is conditioned on the concatenated sequence of the projected image features
 e_{img} and the text prompt embeddings e_{prompt} : $u_{out} = LM_\theta([e_{img}; e_{prompt}])$

155 To obtain the dynamic visual information and motion priors of the input image, we employ another
 156 component to encode it:
 157

- 158 • **Generative Encoder.** We utilize Stable Video Diffusion (SVD) (Blattmann et al., 2023)
 159 as our encoder. SVD consists of a VAE (Kingma & Welling, 2022) encoder ϕ and a U-
 160 Net (Ronneberger et al., 2015) denoiser f_θ . The input image x_{img} is first encoded by VAE
 161 into a latent z_0 , which is then replicated T times to form an initial video latent Z_0 . A single
 Euler integration step is then applied to yield an updated latent $Z_1 = Z_0 + \Delta\sigma f_\theta(Z_0, \sigma_0, c)$.

162 Rather than rendering video frames, the final output $D_{img} = \text{Hidden}^{\text{pre-mid}}(f_\theta, Z_1)$ is
 163 extracted from the U-Net’s pre-middle block.
 164

165 As is shown in Fig. 2, semantic features p_{img} and dynamic features \tilde{H} are projected by two sep-
 166 arate projectors P_{sem} and P_{dyn} into the LLM space, yielding $V_s = P_{\text{sem}}(p_{img}) \in \mathbb{R}^{L_s \times d}$ and
 167 $V_d = P_{\text{dyn}}(\tilde{H}) \in \mathbb{R}^{L_d \times d}$. The fused sequence is $V = [V_s; V_d] \in \mathbb{R}^{(L_s+L_d) \times d}$, which, together
 168 with prompt embeddings E_{prompt} , is fed into the LLM backbone to autoregressively generate an-
 169 swer tokens $u_{out} = \text{LM}_\theta([V; E_{\text{prompt}}])$. By fusing both streams, our WorldLM leverages static
 170 semantics (from SigLIP) and dynamics-aware priors (from SVD) for multimodal reasoning.
 171

172 **Training recipe.** We adopt the training strategy from Prismatic-VLMs (Karamcheti et al., 2024)
 173 using a single-stage training to align modalities and incorporate generative latents: We jointly train
 174 both the projectors and the LLM on a mixture of multimodal instruction datasets from LLaVA-
 175 1.5 (Liu et al., 2023b), together with examples from established vision-language benchmarks (e.g.,
 176 GQA (Hudson & Manning, 2019), TextCaps (Sidorov et al., 2020)), and language-only samples
 177 from ShareGPT (sha). This training paradigm not only effectively aligns the generative encoder’s
 178 representations with the semantic space of the language backbone but also improves the model’s
 179 compositional generalization, enabling it to reason over both motion priors and static features. Re-
 180 markably, the entire training process completes in only 10.3 hours on $16 \times \text{A800}$ GPUs (≈ 165 GPU-
 181 hours) while achieving competitive performance, underscoring the efficiency of our approach.
 182

182 **Inference Protocol** During inference, we employ SigLIP-so400m-patch14-224 as the semantic
 183 vision encoder and Stable Video Diffusion as the generative encoder, with the image resolution set
 184 to 448×448 . As shown in Fig. 2, or K input images, we allocate key frames using evenly spaced
 185 indices within the T -frame latent tensor, replace the corresponding slots with encoded keyframes
 186 before the Euler step, and reuse the resulting latents as additional visual tokens. For the semantic
 187 vision encoder, only the first input image is encoded and concatenated with the input of the genera-
 188 tive encoder. Unless otherwise specified, the number of frames (T) is set to 8 for both single-image
 189 and multi-image inputs.
 190

190 Following the proposed framework, training setup, and inference principles, we train a family of
 191 WorldLM models and designate the ones excelling in **Dynamic Vision Alignment** as **DyVA**.
 192

194 3 PARADIGM COMPARISON

196 Do WorldLM Encoders Entail Visual Semantics Understanding?

198 In this section, we explore how world model latents can benefit visual understanding by contrasting
 199 two differentiating encoder paradigms: (i) traditional static encoders such as CLIP and SigLIP that
 200 prioritize multi-modal semantic alignment, and (ii) world-model encoders based on video generation
 201 models that generate dynamics-aware latents. We begin by comparing the most intuitive design to
 202 test if WorldLMs can work, by directly replacing the CLIP vision encoder of LLaVA 1.5 (Liu et al.,
 203 2024) with a Generative Encoder(e.g., SVD) following the WorldLM pipeline settings in Fig. 2.
 204

204 Generative encoders exhibit fundamentally different performance.

205 We begin with a motivating case study, as illustrated in Fig. 3. Models leveraging static encoders,
 206 such as LLaVA, adopt a *reasoning* paradigm. The output of LLaVA tends to be more descriptive,
 207 describing in depth the details of the given image input. WorldLM, on the other hand, employs
 208 an *envisioning* paradigm, not only encodes the current state of the image, but it also performs a
 209 prediction of plausible (e.g., “will drive away”, and “drive to the other rover”). This case reveals
 210 an inherent difference between the two paradigms: This case reveals an intrinsic difference between
 211 the two paradigms: VLM reasons by the given image’s embeddings, whereas WorldLM attends to
 212 depict the embeddings of generated predictions.
 213

213 **Multi-frame capture more useful semantic features than Single Frame.** The quantitative 3 com-
 214 parison between using different numbers of generated dynamic latents shows its effect on down-
 215 stream tasks. When the generated frames of the video prediction model increase from 1 to 14, we
 see a general increasing trend.

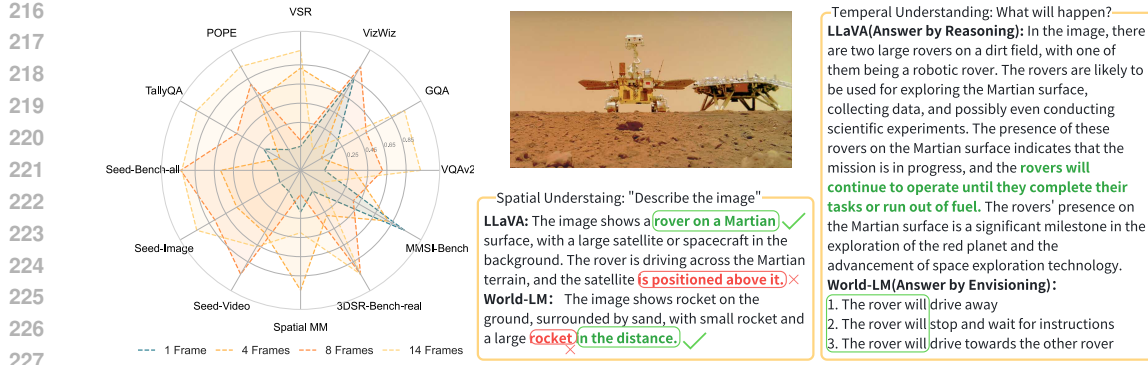


Figure 3: **Paradigm Comparison.** Using the most straightforward setup of WorldLM, we evaluate the impact of predicting 1, 4, 8, and 14 frames. The radar chart demonstrates that increasing the number of frames consistently boosts performance across various vision-language tasks, especially in spatial and temporal reasoning benchmarks such as *SeedBench*, *VSR*, and *TallyQA*. The qualitative example further illustrates that under the same configuration, our WorldLM exhibits a distinct reasoning paradigm by envisioning—offering more concise descriptions, stronger spatial grounding, and more structured temporal foresight compared to LLaVA’s reasoning methods.

Meanwhile, it performs great on spatial-reasoning tasks. Notably, the gains are most pronounced on benchmarks demanding sophisticated spatio-temporal reasoning, such as *SeedBench*, *VSR*, and *TallyQA*. WorldLM’s generative encoders do entail visual understanding, especially in spatio-temporal reasoning. This demonstrates the potential of using world models as dynamics-aware encoders to allow VLMs with a deeper, more grounded level of spatial understanding.

Limitations of WorldLMs. Despite the clear advantages in temporal reasoning, our analysis reveals a critical trade-off. The case study in Figure 3 offers a qualitative explanation for this phenomenon. While our world model correctly grounds the spatial structure of the scene (e.g., “rocket on the ground... large rocket in the distance”), it hallucinates the semantic identity of the objects, misidentifying the Mars lander and rover as “rockets”. Therefore, we believe that using a world model as an encoder has the potential to enhance predictive and spatial reasoning tasks, but requires further improvement to ensure basic semantic capabilities.

4 BENCHMARK ANALYSIS: INVESTIGATION

4.1 EXPERIMENTAL SETUP

We document the configurations, datasets, and training protocols underlying our study. Unless otherwise noted, all settings use a 7B-parameter LLaMA-2 LLM backbone, with both SigLIP and SVD encoders frozen during a single-stage instruction tuning. Training updates are restricted to lightweight projection layers and the language backbone.

4.2 DATASETS AND EVALUATION TARGETS

Benchmarks vary widely in their emphasis on *spatial grounding*, *temporal coherence*, and *semantic understanding*. To assess these dimensions, we curate a suite of open-source **out-of-domain (OOD)** datasets on which our models have not been trained. This allows us to isolate the transferability of world-model priors.

Single-image spatial reasoning. We evaluate on benchmarks that probe relational and spatial understanding without temporal context, including VSR (Liu et al., 2023a), TallyQA (Acharya et al., 2018), SpatialMM-Obj (Shiri et al., 2024), and 3DSR-Bench-real (Ma et al., 2025). Baselines include LLaVA-1.5 (Liu et al., 2024), Prism-SigLIP-7B (Karamchetti et al., 2024), and Prism-DinoSigLIP-7B (Karamchetti et al., 2024).

270 **Multi-image and temporal reasoning.** To assess robustness to sequential inputs and temporal
 271 structure, we use MMSI-Bench (Yang et al., 2025a), SAT-Synthetic (Ray et al., 2024), and Mind-
 272 Cube (Yin et al., 2025). These benchmarks require models to integrate cues across frames or view-
 273 points, testing whether world-model latents can enable multi-frame reasoning. We compare against
 274 both open-source and proprietary large-scale VLMs, including Qwen-2.5-VL-7B (Bai et al., 2025),
 275 InternVL-2.5-7B (Chen et al., 2025), LLaVA-OneVision-7B (Li et al., 2024), and GPT-4o (OpenAI
 276 et al., 2024). Note that all of the compared benchmarks are trained with multi-frame or video data,
 277 whereas we train on single images only.

279 4.3 EXPERIMENTAL ANALYSIS AND INSIGHTS

282 Table 1: Performance comparison between DyVA and state-of-the-art methods on multi-image
 283 benchmarks SAT Synthetic, MMSI-Bench, and MindCube. DyVA outperforms baselines in these
 284 Out-of-Domain tasks. The highest average values are in bold.

285 Model	286 SAT Synthetic						287 MindCube			
	288 Obj Move.	289 Act. Seq.	290 Act. Cons.	291 Goal Aim	292 Persp.	293 Avg.	294 Rot.	295 Among	296 Around	297 Avg.
298 Qwen2.5-VL-7B	299 79.29	300 84.70	301 47.83	302 25.84	303 35.17	304 53.16	305 38.76	306 29.50	307 21.35	308 29.26
309 Intern2.5-VL-8B	310 77.74	311 55.49	312 53.74	313 15.03	314 32.61	315 48.06	316 18.68	317 36.45	318 18.20	319 18.68
320 LLaVA-OneVision-7B	321 71.10	322 21.64	323 49.85	324 31.76	325 35.43	326 43.24	327 36.45	328 48.42	329 44.09	330 47.43
331 GPT-4o	332 61.50	333 33.20	334 47.60	335 67.50	336 37.50	337 49.40	338 40.17	339 29.16	340 38.81	341 38.81
342 DyVA-7B	343 49.15	344 57.81	345 49.25	346 53.38	347 40.44	348 49.51	349 37.70	350 43.10	351 49.00	352 44.62
353 DyVA-Qwen2.5-7B	354 78.83	355 62.13	356 49.85	357 51.86	358 41.72	359 55.24	360 37.20	361 39.10	362 51.70	363 49.80

292 Model	293 MMSI-Bench									
	294 Positional Relationship						295 Attribute		296 Motion	
299	300 Cam-Cam	301 Obj-Obj	302 Reg-Reg	303 Cam-Obj	304 Obj-Reg	305 Cam-Reg	306 Means	307 Appr	308 Cam	309 Obj
310 Qwen2.5-VL-7B	311 32.3	312 27.7	313 29.6	314 32.6	315 24.7	316 32.5	317 26.6	318 27.3	319 16.2	320 31.6
321 Intern2.5-VL-8B	322 24.7	323 24.5	324 24.7	325 25.6	326 29.4	327 26.5	328 25.0	329 18.2	330 20.3	331 39.5
332 LLaVA-OneVision-7B	333 20.4	334 33.0	335 29.6	336 29.1	337 25.9	338 30.1	339 29.7	340 25.8	341 18.9	342 34.2
343 GPT-4o	344 34.4	345 24.5	346 23.5	347 19.8	348 37.6	349 27.7	350 32.8	351 31.8	352 35.1	353 36.8
354 DyVA-7B	355 21.5	356 30.9	357 25.9	358 31.4	359 27.1	360 20.5	361 35.9	362 24.2	363 13.5	364 19.7
365 DyVA-Qwen2.5-7B	366 15.1	367 33.0	368 25.9	369 33.7	370 35.3	371 30.1	372 32.8	373 25.8	374 17.6	375 27.6

300 Tab. 1 and 2 present representative results under both single- and multi-image settings. This framing
 301 allows us to disentangle how world-model features contribute across different reasoning regimes.

302 As presented in Tab. 1 and 2, we evaluate the OOD performance of DyVA-LLaMA-7B and DyVA-
 303 Qwen-2.5-7B. We examine DyVA’s performance relative to existing vision-language models across
 304 various spatial reasoning tasks. The key differences lie in DyVA’s use of “world-model latents”
 305 (SVD-based latent tokens fused with SigLIP image features) versus baselines that use only standard
 306 visual embeddings. Below, we discuss the strengths and weaknesses of DyVA in each benchmark
 307 category, drawing on the reported results and known properties of these tasks and models.

308 The key findings are summarized as follows:

309 **DyVA can enable single-image trained WorldLMs to perform multi-image tasks exceptionally**
 310 **well.** As in Tab. 1, our best variant can perform strongly in multi-frame spatial understanding tasks.

311 Specifically, on the MindCube benchmark (Tab. 1), DyVA-Qwen2.5 achieves a new state-of-the-art
 312 performance with the highest overall score (49.8% vs. 47.4% for the best baseline). It particularly
 313 excels in “Around” (rotating viewpoint) tasks (51.7% vs. 44.1%) and matches or slightly exceeds
 314 baselines on “Rot” tasks (37% vs. 36%). This result suggests that DyVA latents significantly aid
 315 in tasks requiring mental rotation and perspective-taking, likely because they encode cross-view
 316 consistency—the world model inherently “knows” how an object appears from different angles.

317 This achievement is especially noteworthy considering the training efficiency. Compared to base-
 318 lines, LlaVA-One-Vision is trained on 4M multiframe images. Intern 2.5-VL is pretrained with
 319 16.3M samples, including multi-image and video data. Qwen-2.5-VL is also pre-trained with a vari-
 320 ety of data comprising videos and multi-images. These baselines also have several complex methods
 321 for image preprocessing, such as patchifying (Li et al., 2024), processing at different fps (Bai et al.,
 322 2025), and high-res processing (Chen et al., 2025). In stark contrast, we trained our DyVA model
 323 using only the most basic processing methods and a minimalistic data mixture.

324
 325 Table 2: Performance comparison of DyVA variants against baselines on various single-image
 326 spatial reasoning benchmarks, including VSR, TallyQA, SpatialMM-Obj, and 3DSR-Bench-real.
 327 These are Out-of-Domain tasks where models are not trained and perform zero-shot inference. Our
 328 results surpass all baseline models, indicating an improved spatial-reasoning capability from world-
 329 model predicted dynamics. Highest values are highlighted in bold.

330 Models	331 Data	332 VSR							
		333 Topo.	334 Prox.	335 Proj.	336 Direc.	337 Adj.	338 Orien.	339 Unall.	340 Avg.
341 LLaVA-v1.5-7B	342 558k+665k	343 52.24	344 50.00	345 54.77	346 50.00	347 50.86	348 48.98	349 57.50	350 52.94
351 Prism-SigLIP-7B	352 665k	353 67.48	354 62.50	355 65.63	356 66.67	357 55.17	358 55.10	359 67.50	360 64.97
361 Prism-DinoSigLIP-7B	362 665k	363 71.34	364 59.38	365 65.63	366 64.29	367 53.45	368 48.98	369 52.50	370 65.46
371 DyVA-7B	372 665k	373 68.90	374 68.75	375 66.74	376 66.67	377 66.38	378 61.22	379 57.50	380 67.10
381 DyVA-Qwen2.5-7B	382 665k	383 66.67	384 71.88	385 68.74	386 61.90	387 62.93	388 40.82	389 55.00	390 65.63

337 Models	338 Avg.	339 TallyQA			340 SpatialMM-Obj		341 3DSR-Bench-real			
		342 1-obj	343 2-obj	344 Avg.	345 H.	346 L.	347 O.	348 M.	349 Avg.	
350 LLaVA-v1.5-7B	351 58.74	352 57.37	353 44.87	354 48.91	355 55.42	356 57.82	357 26.09	358 39.42	359 45.02	
360 Prism-SigLIP-7B	361 62.25	362 62.54	363 46.77	364 51.86	365 52.28	366 60.22	367 27.23	368 42.17	369 46.55	
370 Prism-DinoSigLIP-7B	371 62.93	372 58.56	373 47.72	374 51.22	375 56.85	376 59.42	377 27.23	378 38.97	379 45.82	
380 DyVA-7B	381 59.47	382 54.78	383 46.29	384 49.03	385 53.71	386 57.60	387 27.23	388 40.80	389 45.41	
390 DyVA-Qwen2.5-7B	391 68.11	392 62.74	393 47.53	394 52.44	395 52.57	396 54.51	397 27.23	398 49.60	399 47.16	

345
 346
 347 Our modest training budget and intuitive multi-image inference method suggest that world model
 348 latents strongly enhance the spatial understanding on multi-image benchmarks. We also believe that
 349 the fusion of SVD with SigLIP is a key factor that directly improves multi-image reasoning abilities.

350 **DyVA excels in handling spatial relations, counting and object queries, and 3D Scenes.** In
 351 Single-Image Spatial Reasoning, DyVA’s world-model features boost performance on tasks em-
 352 phasizing geometric and relational spatial reasoning (orientation, adjacency, multi-object spatial
 353 layouts), reflecting improved 3D awareness.

354
 355 1. Visual Spatial Relations (VSR): DyVA-LLaMA (SigLIP+SVD) achieves the highest average
 356 score (67.1%) across VSR subtasks (topology, proximity, projection, direction, adjacency, orien-
 357 tation, unaligned), outperforming the SigLIP-only baselines (64.9–65.5%) Tab. 2. In particular,
 358 DyVA significantly improves orientation reasoning (61.2% vs 55–49% for baselines) and prox-
 359 imity/topology, suggesting world-model latents better encode spatial layouts and object alignment.
 360 However, DyVA falls behind on the “Unaligned” subtask (57.5% vs 67.5% for Prism-SigLIP), indi-
 361 cating that embedding world-model context can hurt when objects lack canonical alignments (per-
 362 haps because the latent prior biases toward canonical scene structures).

363
 364 2. Counting and Object Queries (TallyQA, SpatialMM-Obj): On TallyQA (visual counting),
 365 DyVA-Qwen2.5 excels (68.1% average), well above Prism baselines (62–63%) and LLaVA
 366 (58.7%)Tab. 2. This suggests the latents help Qwen2.5 better aggregate multi-object cues needed
 367 for counting. Interestingly, DyVA-LLaMA does not show the same gain (59.5%), implying that ef-
 368 fective use of SVD features depends on backbone capacity. For the SpatialMM-Obj task (single- vs
 369 multi-object queries), DyVA-Qwen2.5 again slightly outperforms others (52.4% vs 51.8% baseline)
 370 on the combined 1- and 2-object questions.

371
 372 3. 3D Scene Reasoning (3DSR-Bench-real): This benchmark measures 3D spatial and depth
 373 understanding in real images. Notably, DyVA greatly improves the “Multiple objects” (M) subset
 374 (49.6% vs 40% for baselines). This aligns with the idea that SVD latents capture implicit depth and
 375 occlusion cues learned from video/world modeling

376
 377 **Limitations and Areas for Improvement.** Despite its strengths in spatial reasoning, DyVA exhibits
 378 certain limitations, particularly on tasks that rely heavily on semantic language priors, non-canonical
 379 object arrangements, or temporal sequence understanding.

380
 381 1. Weakened Performance on Language-Intensive Tasks: The fusion of world-model tokens can
 382 dilute the semantic precision required for certain tasks. On benchmarks like VQAv2 and TextVQA,

378 which demand strong language priors and OCR capabilities, DyVA underperforms compared to
 379 SigLIP-only baselines. This suggests that while SVD latents enhance spatial awareness, they can in-
 380 terfere with fine-grained semantic grounding and text recognition where the original visual features
 381 are more direct and precise.

382 2. Bias Towards Canonical Scene Structures: As previously noted in the VSR analysis, DyVA’s
 383 performance drops significantly on the “Unaligned” subtask (57.5% vs. 67.5%). This indicates
 384 that embedding world-model context can be detrimental when objects lack canonical alignments.
 385 The model’s latent prior appears biased toward common or expected scene structures, hindering its
 386 ability to reason about novel or unusual spatial configurations.

387 3. Less Reliable Sequential and Temporal Reasoning: The current SVD latents are less effective for
 388 understanding dynamic sequences. This is evidenced by a large performance drop in SAT Action
 389 Sequence and mixed results on MMSI. These outcomes suggest that the latents, while powerful for
 390 static scenes, are less reliable for predicting discrete action orders or interpreting rapid changes over
 391 time, marking a clear area for future improvement.

393 394 5 DESIGN-SPACE EXPLORATION: WHY DYVA WORKS?

395 Building on the strong spatial performance demonstrated in both single-image and multi-image tasks
 396 in our experiments, we further analyze two key design axes to investigate the sources of WorldLM’s
 397 benefits: (i) the choice of different semantic vision encoders, and (ii) the potential of leveraging
 398 text-loss to jointly supervise the training of the VAE and U-Net.

400
 401 **Table 3: Performance Comparison of SVD-based Vision Models.** Benchmark scores across a suite
 402 of VQA, reasoning, and spatio-temporal tasks. All experiments use the LLaMA-2 7B backbone. The highest
 403 score in each column is marked in **bold**, and the second-highest is underlined. Align: one-time alignment on
 404 LAION-558k. F1: one-time finetuning. Fused: 3-layer MLP projector.

Model	Align	VQAv2	GQA	VizWiz	VSR	POPE	TallyQA	SeedBench	SpatialMM	3DSR
VAE-Only	✗	46.98	40.53	38.90	52.04	66.42	39.55	38.18	38.81	44.15
	✓	50.70	43.26	48.67	52.29	60.80	42.48	41.53	37.3	43.43
SVD-Only	✗	63.51	55.18	44.95	57.93	82.38	49.75	50.15	42.03	42.93
	✓	61.82	50.20	50.60	53.60	75.61	53.27	52.55	40.60	43.50
U-Net Trainable	✓	63.36	54.49	50.24	57.93	79.88	51.51	52.76	40.80	43.43
U-Net & VAE Trainable	✓	60.99	49.80	50.17	52.53	77.08	53.75	52.33	39.50	44.00
Dino + SVD	✗	68.77	58.50	50.73	62.52	85.25	52.78	55.19	44.79	44.26
	✓	68.44	55.57	51.13	59.41	85.54	54.15	56.49	43.40	45.07
SigLIP + SVD	✗	75.36	61.52	55.95	67.10	85.97	59.47	66.61	49.03	45.40
	✓	73.63	58.89	54.63	61.62	84.37	56.98	62.09	45.40	45.49
U-Net Trainable	✓	74.02	59.86	54.60	62.27	85.61	57.42	63.39	45.95	44.11
CLIP + SVD	✗	73.51	59.67	53.14	64.89	85.80	<u>58.25</u>	<u>65.45</u>	46.07	46.13
	✓	72.99	60.74	<u>55.89</u>	<u>65.38</u>	85.80	55.37	65.33	46.70	44.42
DinoSigLIP + SVD	✗	<u>74.28</u>	60.16	54.13	64.81	87.27	57.42	64.54	<u>48.65</u>	44.15
	✓	72.42	59.28	54.47	61.29	<u>86.75</u>	54.98	61.54	47.00	45.14

418 419 5.1 WHY DO VAE, DINO, SVD-ONLY NOT WORK, BUT SIGLIP+SVD DOES?

420 To investigate the respective roles of the generative encoder and the semantic vision encoder within
 421 WorldLM, we conducted a two-stage ablation study: **First**, in a setting without the semantic vision
 422 encoder, we decoupled the generative encoder into its constituent VAE and the complete generative
 423 encoder architecture. We then trained and comparatively evaluated the performance of two distinct
 424 encoding approaches: one employing only the VAE for encoding and the other utilizing the entire
 425 generative encoder (SVD). **Second**, while keeping the generative encoder fixed, we systematically
 426 substituted the backbone of the semantic vision encoder with various alternative architectures to
 427 analyze its impact on the model’s overall performance.

428 Our quantitative experimental results are presented in Tab. 3. Furthermore, to provide a more intu-
 429 itive visualization and comparison of the performance of different encoders.

430 **Prediction Matters.** The inference protocol for the SVD encoder has been detailed in Sec. 2. A
 431 similar inference process is employed when using the VAE as the generative encoder. In contrast to

432 extracting features from the pre-middle block of the U-Net, we directly use the features encoded by
 433 the VAE. To align the feature dimensionality with that of the SVD, we prepend several convolutional
 434 layers to the projector. As evidenced by our experimental results in Tab. 3, the model employing only
 435 VAE for encoding exhibits a performance degradation across nearly all benchmarks when compared
 436 to models using SVD. This finding underscores the significance of the predicted dynamics for the
 437 WorldLM.

438 **WorldLM needs a text-aligned encoder.** Although SigLIP (Zhai et al., 2023) has recently shown
 439 dominant performance as an emerging vision encoder in current state-of-the-art VLMs, such as
 440 LLaVA-One-Vision (Li et al., 2024) and Prismatic-VLM (Karamchetti et al., 2024), in this study,
 441 we investigate the respective roles of SigLIP, CLIP (Radford et al., 2021), DINOv2 (Oquab et al.,
 442 2024), and a combined DINO-SigLIP architecture as the semantic vision encoder. To ensure a fair
 443 comparison, we selected the ViT-L version for each model, all configured for a 224×224 input
 444 resolution. Furthermore, we adopted a consistent image processing strategy, which involves scaling
 445 and then cropping all images to these uniform resolutions.

446 As demonstrated in Tab. 3, models that utilize SigLIP (including the DINO-SigLIP combination)
 447 or CLIP as the semantic vision encoder significantly outperform the model using DINOv2. Fur-
 448 thermore, when considering the aforementioned investigation of the generative encoder, the model
 449 with DINOv2 as the semantic vision encoder, in turn, shows better performance than the generative-
 450 encoder-only architecture.

451 This leads to a key insight: for our WorldLM framework that is trained under the text-loss su-
 452 pervision, in addition to the predicted dynamic features, it requires supplementary visual-semantic
 453 information from a model pre-trained on language-vision tasks (i.e., a text-aligned model). This in-
 454 sight also paves the way for future explorations: Can the generative encoder alone suffice to replace
 455 the semantic vision encoder? Could the performance be further improved by replacing the VAE?
 456 And is text-loss supervision the answer to WorldLM training?

457

458 5.2 CAN DYVA BENEFIT FROM U-NET & VAE TRAINING ON TEXT-LOSS?

459

460 We investigated the efficacy of fine-tuning the SVD’s core components (U-Net and VAE) using only
 461 a text-loss signal. Our experimental results indicate this strategy is largely ineffective.

462 **Text supervision failed to help VQA tasks.** As shown in Tab. 3, making only the U-Net trainable
 463 yields inconsistent and marginal performance changes, while allowing both the U-Net and VAE to
 464 be trainable leads to a distinct and widespread degradation in performance across the benchmarks.

465 This suggests the high-level semantic supervision from the text-loss is ill-suited for adapting the low-
 466 level generative priors of these components. This constitutes one of the limitations of our current
 467 work. An alternative approach, inspired by methods like RAPE-E (Leng et al., 2025), involves
 468 aligning the features from the VAE and U-Net with the visual features from a semantic encoder such
 469 as DINOv2. Exploring such an alignment strategy is a promising direction for future research.

470

471

472 6 DISCUSSIONS AND OUTLOOKS

473

474 **(1)** Paradigm comparisons reveal that world-model latents are powerful: generated frame latents un-
 475 lock spatial and multi-view reasoning, yet can erode fidelity and increase hallucination. **(2)** Design-
 476 space sweeps clarify which architectural choices mitigate these effects, while benchmark diagnostics
 477 explain when each paradigm wins. **(3)** Open directions include aligning SVD tokens with textual
 478 references, adaptive frame selection, and attention regularizers that maintain semantic grounding
 479 while exploiting the structure of the world model. **(4)** World Model is a powerful visual encoder:
 480 The key concept of WorldLM is using the prediction pretraining to enhance the spatial-temporal
 481 understanding ability of the general VLM. Though DyVA achieves SOTA performance, one signif-
 482 icant weakness still remains: its prediction feature relies on the worst-performing encoder, VAE.
 483 Therefore, the world model can be more deeply explored, instead of using SVD, design a world
 484 model closer to the language latent space, for understanding tasks. For example, use SigLIP to train
 485 a SigLIP world model by Joint-Embedding-Prediction-Architecture. Furthermore, we argue that us-
 486 ing a prediction model as an encoder might be a potential new paradigm for more broader domain,
 487 across robotics, visual-language understanding, and to more general visual understanding.

486 REFERENCES
487488 Sharegpt: Share your wildest chatgpt conversations with one click. <https://sharegpt.com/>.489
490 Manoj Acharya, Kushal Kafle, and Christopher Kanan. Tallyqa: Answering complex counting
491 questions, 2018. URL <https://arxiv.org/abs/1810.12440>.492
493 Pablo Acuaviva, Aram Davtyan, Mariam Hassan, Sebastian Stapf, Ahmad Rahimi, Alexandre Alahi,
494 and Paolo Favaro. From generation to generalization: Emergent few-shot learning in video diffu-
495 sion models, 2025. URL <https://arxiv.org/abs/2506.07280>.496
497 Niket Agarwal, Arslan Ali, Maciej Bala, Yogesh Balaji, Erik Barker, Tiffany Cai, Prithvijit Chat-
498 topadhyay, Yongxin Chen, Yin Cui, Yifan Ding, Daniel Dworakowski, Jiaoqiao Fan, Michele
499 Fenzi, Francesco Ferroni, Sanja Fidler, Dieter Fox, Songwei Ge, Yunhao Ge, Jinwei Gu, Sid-
500 dharth Gururani, Ethan He, Jiahui Huang, Jacob Huffman, Pooya Jannaty, Jingyi Jin, Seung Wook
501 Kim, Gergely Klár, Grace Lam, Shiyi Lan, Laura Leal-Taixé, Anqi Li, Zhaoshuo Li, Chen-
502 Hsuan Lin, Tsung-Yi Lin, Huan Ling, Ming-Yu Liu, Xian Liu, Alice Luo, Qianli Ma, Hanzi
503 Mao, Kaichun Mo, Arsalan Mousavian, Seungjun Nah, Sriharsha Niverty, David Page, Despoina
504 Paschalidou, Zeeshan Patel, Lindsey Pavao, Morteza Ramezanali, Fitsum Reda, Xiaowei Ren,
505 Vasanth Rao Naik Sabavat, Ed Schmerling, Stella Shi, Bartosz Stefanik, Shitao Tang, Lyne
506 Tchapmi, Przemysław Tredak, Wei-Cheng Tseng, Jibin Varghese, Hao Wang, Haoxiang Wang,
507 Heng Wang, Ting-Chun Wang, Fangyin Wei, Xinyue Wei, Jay Zhangjie Wu, Jiashu Xu, Wei Yang,
508 Lin Yen-Chen, Xiaohui Zeng, Yu Zeng, Jing Zhang, Qinsheng Zhang, Yuxuan Zhang, Qingqing
509 Zhao, and Artur Zabkowski. Cosmos world foundation model platform for physical ai. *CoRR*,
510 abs/2501.03575, 2025a. doi: 10.48550/arXiv.2501.03575.511
512 Niket Agarwal, Arslan Ali, Maciej Bala, Yogesh Balaji, Erik Barker, Tiffany Cai, Prithvijit Chat-
513 topadhyay, Yongxin Chen, Yin Cui, Yifan Ding, et al. Cosmos world foundation model platform
514 for physical ai. *arXiv preprint arXiv:2501.03575*, 2025b.515
516 Mido Assran, Adrien Bardes, David Fan, Quentin Garrido, Russell Howes, Mojtaba Komeili,
517 Matthew J. Muckley, Ammar Rizvi, Claire Roberts, Koustuv Sinha, Artem Zholus, Sergio Ar-
518 naud, Abha Gejji, Ada Martin, François R. Hogan, Daniel Dugas, Piotr Bojanowski, Vasil Khali-
519 dov, Patrick Labatut, Francisco Massa, Marc Szafraniec, Kapil Krishnakumar, Yong Li, Xiaodong
520 Ma, Sarath Chandar, Franziska Meier, Yann LeCun, Michael Rabbat, and Nicolas Ballas. V-
521 jepa 2: Self-supervised video models enable understanding, prediction and planning. *CoRR*,
522 abs/2506.09985, 2025. doi: 10.48550/arXiv.2506.09985.523
524 Shuai Bai, Keqin Chen, Xuejing Liu, Jialin Wang, Wenbin Ge, Sibo Song, Kai Dang, Peng Wang,
525 Shijie Wang, Jun Tang, Humen Zhong, Yuanzhi Zhu, Mingkun Yang, Zhaohai Li, Jianqiang Wan,
526 Pengfei Wang, Wei Ding, Zheren Fu, Yiheng Xu, Jiabo Ye, Xi Zhang, Tianbao Xie, Zesen Cheng,
527 Hang Zhang, Zhibo Yang, Haiyang Xu, and Junyang Lin. Qwen2.5-vl technical report, 2025.
528 URL <https://arxiv.org/abs/2502.13923>.529
530 Yutong Bai, Xinyang Geng, Karttikeya Mangalam, Amir Bar, Alan L. Yuille, Trevor Darrell, Jiten-
531 dra Malik, and Alexei A. Efros. Sequential modeling enables scalable learning for large vision
532 models. *arXiv preprint arXiv:2312.00785*, 2024. doi: 10.48550/arXiv.2312.00785.533
534 Andreas Blattmann, Tim Dockhorn, Sumith Kulal, Daniel Mendelevitch, Maciej Kilian, Dominik
535 Lorenz, Yam Levi, Zion English, Vikram Voleti, Adam Letts, Varun Jampani, and Robin Rom-
536 bach. Stable video diffusion: Scaling latent video diffusion models to large datasets. *CoRR*,
537 abs/2311.15127, 2023. doi: 10.48550/arXiv.2311.15127.538
539 Mathilde Caron, Hugo Touvron, Ishan Misra, Hervé Jégou, Julien Mairal, Piotr Bojanowski, and
540 Armand Joulin. Emerging properties in self-supervised vision transformers, 2021. URL <https://arxiv.org/abs/2104.14294>.541
542 Xinyan Chen*, Renrui Zhang*, Dongzhi Jiang, Aojun Zhou, Shilin Yan, Weifeng Lin, and Hong-
543 sheng Li. Mint-cot: Enabling interleaved visual tokens in mathematical chain-of-thought reason-
544 ing. *arXiv preprint arXiv:2506.05331*, 2025.

540 Zhe Chen, Weiyun Wang, Yue Cao, Yangzhou Liu, Zhangwei Gao, Erfei Cui, Jinguo Zhu, Shen-
 541 glong Ye, Hao Tian, Zhaoyang Liu, Lixin Gu, Xuehui Wang, Qingyun Li, Yimin Ren, Zixuan
 542 Chen, Jiapeng Luo, Jiahao Wang, Tan Jiang, Bo Wang, Conghui He, Botian Shi, Xingcheng
 543 Zhang, Han Lv, Yi Wang, Wenqi Shao, Pei Chu, Zhongying Tu, Tong He, Zhiyong Wu, Huipeng
 544 Deng, Jiaye Ge, Kai Chen, Kaipeng Zhang, Limin Wang, Min Dou, Lewei Lu, Xizhou Zhu,
 545 Tong Lu, Dahua Lin, Yu Qiao, Jifeng Dai, and Wenhui Wang. Expanding performance bound-
 546 aries of open-source multimodal models with model, data, and test-time scaling, 2025. URL
 547 <https://arxiv.org/abs/2412.05271>.

548 Alexey Dosovitskiy, Lucas Beyer, Alexander Kolesnikov, Dirk Weissenborn, Xiaohua Zhai, Thomas
 549 Unterthiner, Mostafa Dehghani, Matthias Minderer, Georg Heigold, Sylvain Gelly, Jakob Uszko-
 550 reit, and Neil Houlsby. An image is worth 16x16 words: Transformers for image recognition at
 551 scale, 2021. URL <https://arxiv.org/abs/2010.11929>.

552 Zigang Geng, Binxin Yang, Tiankai Hang, Chen Li, Shuyang Gu, Ting Zhang, Jianmin Bao, Zheng
 553 Zhang, Han Hu, Dong Chen, and Baining Guo. Instructdiffusion: A generalist modeling interface
 554 for vision tasks. *CoRR*, abs/2309.03895, 2023. doi: 10.48550/arXiv.2309.03895.

555 Ziyu Guo*, Renrui Zhang*, Xiangyang Zhu, Yiwen Tang, Xianzheng Ma, Jiaming Han, Kexin
 556 Chen, Peng Gao, Xianzhi Li, Hongsheng Li, et al. Point-bind & point-llm: Aligning point cloud
 557 with multi-modality for 3d understanding, generation, and instruction following. *arXiv preprint*
 558 *arXiv:2309.00615*, 2023.

559 Ziyu Guo*, Renrui Zhang*, Chengzhuo Tong*, Zhizheng Zhao*, Peng Gao, Hongsheng Li, and
 560 Pheng-Ann Heng. Can we generate images with cot? let's verify and reinforce image generation
 561 step by step. *CVPR 2025*, 2025.

562 David Ha and Jürgen Schmidhuber. World models. *CoRR*, abs/1803.10122, 2018. doi: 10.48550/
 563 arXiv.1803.10122.

564 Danijar Hafner, Timothy P. Lillicrap, Ian Fischer, Ruben Villegas, David Ha, Honglak Lee, and
 565 James Davidson. Learning latent dynamics for planning from pixels. *CoRR*, abs/1811.04551,
 566 2018. doi: 10.48550/arXiv.1811.04551.

567 Danijar Hafner, Timothy P. Lillicrap, Jimmy Ba, and Mohammad Norouzi. Dream to control: Learn-
 568 ing behaviors by latent imagination. *CoRR*, abs/1912.01603, 2019. doi: 10.48550/arXiv.1912.
 569 01603.

570 Dan Hendrycks and Kevin Gimpel. Gaussian error linear units (gelus), 2023. URL <https://arxiv.org/abs/1606.08415>.

571 Anthony Hu, Lloyd Russell, Hudson Yeo, Zak Murez, George Fedoseev, Alex Kendall, Jamie Shot-
 572 ton, and Gianluca Corrado. Gaia-1: A generative world model for autonomous driving, 2023.
 573 URL <https://arxiv.org/abs/2309.17080>.

574 Drew A. Hudson and Christopher D. Manning. GQA: A new dataset for real-world visual reasoning
 575 and compositional question answering. In *Proceedings of the IEEE/CVF Conference on Computer
 576 Vision and Pattern Recognition (CVPR)*, 2019.

577 Dongsheng Jiang, Yuchen Liu, Songlin Liu, Jin'e Zhao, Hao Zhang, Zhen Gao, Xiaopeng Zhang, Jin
 578 Li, and Hongkai Xiong. From clip to dino: Visual encoders shout in multi-modal large language
 579 models. *arXiv preprint arXiv:2310.08825*, 2023. doi: 10.48550/arXiv.2310.08825.

580 Siddharth Karamcheti, Suraj Nair, Ashwin Balakrishna, Percy Liang, Thomas Kollar, and Dorsa
 581 Sadigh. Prismatic vlms: Investigating the design space of visually-conditioned language models,
 582 2024. URL <https://arxiv.org/abs/2402.07865>.

583 Diederik P Kingma and Max Welling. Auto-encoding variational bayes, 2022. URL <https://arxiv.org/abs/1312.6114>.

584 Xingjian Leng, Jaskirat Singh, Yunzhong Hou, Zhenchang Xing, Saining Xie, and Liang Zheng.
 585 Repa-e: Unlocking vae for end-to-end tuning with latent diffusion transformers, 2025. URL
 586 <https://arxiv.org/abs/2504.10483>.

594 Bo Li, Yuanhan Zhang, Dong Guo, Renrui Zhang, Feng Li, Hao Zhang, Kaichen Zhang, Peiyuan
 595 Zhang, Yanwei Li, Ziwei Liu, and Chunyuan Li. Llava-onevision: Easy visual task transfer, 2024.
 596 URL <https://arxiv.org/abs/2408.03326>.

597 Yijing Lin, Mengqi Huang, Shuhan Zhuang, and Zhendong Mao. Realgeneral: Unifying visual
 598 generation via temporal in-context learning with video models. *arXiv preprint arXiv:2503.10406*,
 599 2025. URL <https://arxiv.org/abs/2503.10406>.

600 Fangyu Liu, Guy Emerson, and Nigel Collier. Visual spatial reasoning. *Transactions of the As-
 601 sociation for Computational Linguistics*, 11:635–651, 2023a. doi: 10.1162/tacl_a_00566. URL
 602 <https://aclanthology.org/2023.tacl-1.37/>.

603 Haotian Liu, Chunyuan Li, Qingyang Wu, and Yong Jae Lee. Visual instruction tuning, 2023b. URL
 604 <https://arxiv.org/abs/2304.08485>.

605 Haotian Liu, Chunyuan Li, Yuheng Li, and Yong Jae Lee. Improved baselines with visual instruction
 606 tuning, 2024. URL <https://arxiv.org/abs/2310.03744>.

607 Wufei Ma, Haoyu Chen, Guofeng Zhang, Yu-Cheng Chou, Jieneng Chen, Celso M de Melo, and
 608 Alan Yuille. 3dsrbench: A comprehensive 3d spatial reasoning benchmark, 2025. URL <https://arxiv.org/abs/2412.07825>.

609 OpenAI. Video generation models as world simulators, 2024. URL <https://openai.com/index/video-generation-models-as-world-simulators/>. Accessed: 2025-09-
 610 10.

611 OpenAI, :, Aaron Hurst, Adam Lerer, Adam P. Goucher, Adam Perelman, Aditya Ramesh, Aidan
 612 Clark, AJ Ostrow, Akila Welihinda, Alan Hayes, Alec Radford, Aleksander Madry, Alex Baker-
 613 Whitcomb, Alex Beutel, Alex Borzunov, Alex Carney, Alex Chow, Alex Kirillov, Alex Nichol,
 614 Alex Paino, Alex Renzin, Alex Tachard Passos, Alexander Kirillov, Alexi Christakis, Alexis Con-
 615 neau, Ali Kamali, Allan Jabri, Allison Moyer, Allison Tam, Amadou Crookes, Amin Tootoochian,
 616 Amin Tootoonchian, Ananya Kumar, Andrea Vallone, Andrej Karpathy, Andrew Braunstein,
 617 Andrew Cann, Andrew Codispoti, Andrew Galu, Andrew Kondrich, Andrew Tulloch, Andrey
 618 Mishchenko, Angela Baek, Angela Jiang, Antoine Pelisse, Antonia Woodford, Anuj Gosalia,
 619 Arka Dhar, Ashley Pantuliano, Avi Nayak, Avital Oliver, Barret Zoph, Behrooz Ghorbani, Ben
 620 Leimberger, Ben Rossen, Ben Sokolowsky, Ben Wang, Benjamin Zweig, Beth Hoover, Blake
 621 Samic, Bob McGrew, Bobby Spero, Bogo Giertler, Bowen Cheng, Brad Lightcap, Brandon
 622 Walkin, Brendan Quinn, Brian Guarraci, Brian Hsu, Bright Kellogg, Brydon Eastman, Camillo
 623 Lugaressi, Carroll Wainwright, Cary Bassin, Cary Hudson, Casey Chu, Chad Nelson, Chak Li,
 624 Chan Jun Shern, Channing Conger, Charlotte Barette, Chelsea Voss, Chen Ding, Cheng Lu,
 625 Chong Zhang, Chris Beaumont, Chris Hallacy, Chris Koch, Christian Gibson, Christina Kim,
 626 Christine Choi, Christine McLeavey, Christopher Hesse, Claudia Fischer, Clemens Winter, Coley
 627 Czarnecki, Colin Jarvis, Colin Wei, Constantin Koumouzelis, Dane Sherburn, Daniel Kappler,
 628 Daniel Levin, Daniel Levy, David Carr, David Farhi, David Mely, David Robinson, David Sasaki,
 629 Denny Jin, Dev Valladares, Dimitris Tsipras, Doug Li, Duc Phong Nguyen, Duncan Findlay,
 630 Edede Oiwoh, Edmund Wong, Ehsan Asdar, Elizabeth Proehl, Elizabeth Yang, Eric Antonow,
 631 Eric Kramer, Eric Peterson, Eric Sigler, Eric Wallace, Eugene Brevdo, Evan Mays, Farzad Kho-
 632 rasani, Felipe Petroski Such, Filippo Raso, Francis Zhang, Fred von Lohmann, Freddie Sulit,
 633 Gabriel Goh, Gene Oden, Geoff Salmon, Giulio Starace, Greg Brockman, Hadi Salman, Haiming
 634 Bao, Haitang Hu, Hannah Wong, Haoyu Wang, Heather Schmidt, Heather Whitney, Heewoo Jun,
 635 Hendrik Kirchner, Henrique Ponde de Oliveira Pinto, Hongyu Ren, Huiwen Chang, Hyung Won
 636 Chung, Ian Kivlichan, Ian O’Connell, Ian O’Connell, Ian Osband, Ian Silber, Ian Sohl, Ibrahim
 637 Okuyucu, Ikai Lan, Ilya Kostrikov, Ilya Sutskever, Ingmar Kanitscheider, Ishaan Gulrajani, Ja-
 638 cob Coxon, Jacob Menick, Jakub Pachocki, James Aung, James Betker, James Crooks, James
 639 Lennon, Jamie Kiros, Jan Leike, Jane Park, Jason Kwon, Jason Phang, Jason Teplitz, Jason Wei,
 640 Jason Wolfe, Jay Chen, Jeff Harris, Jenia Varavva, Jessica Gan Lee, Jessica Shieh, Ji Lin, Jiahui
 641 Yu, Jiayi Weng, Jie Tang, Jieqi Yu, Joanne Jang, Joaquin Quinonero Candela, Joe Beutler, Joe
 642 Landers, Joel Parish, Johannes Heidecke, John Schulman, Jonathan Lachman, Jonathan McKay,
 643 Jonathan Uesato, Jonathan Ward, Jong Wook Kim, Joost Huizinga, Jordan Sitkin, Jos Kraaijveld,
 644 Josh Gross, Josh Kaplan, Josh Snyder, Joshua Achiam, Joy Jiao, Joyce Lee, Juntang Zhuang,
 645 Justyn Harriman, Kai Fricke, Kai Hayashi, Karan Singhal, Katy Shi, Kavin Karthik, Kayla Wood,
 646 647

648 Kendra Rimbach, Kenny Hsu, Kenny Nguyen, Keren Gu-Lemberg, Kevin Button, Kevin Liu, Kiel
 649 Howe, Krithika Muthukumar, Kyle Luther, Lama Ahmad, Larry Kai, Lauren Itow, Lauren Work-
 650 man, Leher Pathak, Leo Chen, Li Jing, Lia Guy, Liam Fedus, Liang Zhou, Lien Mamitsuka,
 651 Lilian Weng, Lindsay McCallum, Lindsey Held, Long Ouyang, Louis Feuvrier, Lu Zhang, Lukas
 652 Kondraciuk, Lukasz Kaiser, Luke Hewitt, Luke Metz, Lyric Doshi, Mada Aflak, Maddie Simens,
 653 Madelaine Boyd, Madeleine Thompson, Marat Dukhan, Mark Chen, Mark Gray, Mark Hudnall,
 654 Marvin Zhang, Marwan Aljubeh, Mateusz Litwin, Matthew Zeng, Max Johnson, Maya Shetty,
 655 Mayank Gupta, Meghan Shah, Mehmet Yatbaz, Meng Jia Yang, Mengchao Zhong, Mia Glaese,
 656 Mianna Chen, Michael Janner, Michael Lampe, Michael Petrov, Michael Wu, Michele Wang,
 657 Michelle Fradin, Michelle Pokrass, Miguel Castro, Miguel Oom Temudo de Castro, Mikhail
 658 Pavlov, Miles Brundage, Miles Wang, Minal Khan, Mira Murati, Mo Bavarian, Molly Lin, Murat
 659 Yesildal, Nacho Soto, Natalia Gimelshein, Natalie Cone, Natalie Staudacher, Natalie Summers,
 660 Natan LaFontaine, Neil Chowdhury, Nick Ryder, Nick Stathas, Nick Turley, Nik Tezak, Niko Fe-
 661 lix, Nithanth Kudige, Nitish Keskar, Noah Deutsch, Noel Bundick, Nora Puckett, Ofir Nachum,
 662 Ola Okelola, Oleg Boiko, Oleg Murk, Oliver Jaffe, Olivia Watkins, Olivier Godement, Owen
 663 Campbell-Moore, Patrick Chao, Paul McMillan, Pavel Belov, Peng Su, Peter Bak, Peter Bakkum,
 664 Peter Deng, Peter Dolan, Peter Hoeschele, Peter Welinder, Phil Tillet, Philip Pronin, Philippe
 665 Tillet, Prafulla Dhariwal, Qiming Yuan, Rachel Dias, Rachel Lim, Rahul Arora, Rajan Troll, Ran-
 666 dall Lin, Rapha Gontijo Lopes, Raul Puri, Reah Miyara, Reimar Leike, Renaud Gaubert, Reza
 667 Zamani, Ricky Wang, Rob Donnelly, Rob Honsby, Rocky Smith, Rohan Sahai, Rohit Ramchan-
 668 dani, Romain Huet, Rory Carmichael, Rowan Zellers, Roy Chen, Ruby Chen, Ruslan Nigmat-
 669 ullin, Ryan Cheu, Saachi Jain, Sam Altman, Sam Schoenholz, Sam Toizer, Samuel Miserendino,
 670 Sandhini Agarwal, Sara Culver, Scott Ethersmith, Scott Gray, Sean Grove, Sean Metzger, Shamez
 671 Hermani, Shantanu Jain, Shengjia Zhao, Sherwin Wu, Shino Jomoto, Shirong Wu, Shuaiqi, Xia,
 672 Sonia Phene, Spencer Papay, Srinivas Narayanan, Steve Coffey, Steve Lee, Stewart Hall, Suchir
 673 Balaji, Tal Broda, Tal Stramer, Tao Xu, Tarun Gogineni, Taya Christianson, Ted Sanders, Tejal
 674 Patwardhan, Thomas Cunningham, Thomas Degry, Thomas Dimson, Thomas Raoux, Thomas
 675 Shadwell, Tianhao Zheng, Todd Underwood, Todor Markov, Toki Sherbakov, Tom Rubin, Tom
 676 Stasi, Tomer Kaftan, Tristan Heywood, Troy Peterson, Tyce Walters, Tyna Eloundou, Valerie Qi,
 677 Veit Moeller, Vinnie Monaco, Vishal Kuo, Vlad Fomenko, Wayne Chang, Weiyi Zheng, Wenda
 678 Zhou, Wesam Manassra, Will Sheu, Wojciech Zaremba, Yash Patil, Yilei Qian, Yongjik Kim,
 Youlong Cheng, Yu Zhang, Yuchen He, Yuchen Zhang, Yujia Jin, Yunxing Dai, and Yury Malkov.
 679 Gpt-4o system card, 2024. URL <https://arxiv.org/abs/2410.21276>.

680 Maxime Oquab, Timothée Darcet, Théo Moutakanni, Huy Vo, Marc Szafraniec, Vasil Khalidov,
 681 Pierre Fernandez, Daniel Haziza, Francisco Massa, Alaaeldin El-Nouby, Mahmoud Assran, Nico-
 682 las Ballas, Wojciech Galuba, Russell Howes, Po-Yao Huang, Shang-Wen Li, Ishan Misra, Michael
 683 Rabbat, Vasu Sharma, Gabriel Synnaeve, Hu Xu, Hervé Jegou, Julien Mairal, Patrick Labatut, Ar-
 684 mand Joulin, and Piotr Bojanowski. Dinov2: Learning robust visual features without supervision,
 685 2024. URL <https://arxiv.org/abs/2304.07193>.

686 Alec Radford, Jong Wook Kim, Chris Hallacy, Aditya Ramesh, Gabriel Goh, Sandhini Agar-
 687 wal, Girish Sastry, Amanda Askell, Pamela Mishkin, Jack Clark, Gretchen Krueger, and Ilya
 688 Sutskever. Learning transferable visual models from natural language supervision. *arXiv preprint*
 689 *arXiv:2103.00020*, 2021. doi: 10.48550/arXiv.2103.00020.

690 Arijit Ray, Jiafei Duan, Reuben Tan, Dina Bashkirova, Rose Hendrix, Kiana Ehsani, Aniruddha
 691 Kembhavi, Bryan A. Plummer, Ranjay Krishna, Kuo-Hao Zeng, and Kate Saenko. Sat: Spatial
 692 aptitude training for multimodal language models. *arXiv preprint arXiv:2412.07755*, 2024.

693 Olaf Ronneberger, Philipp Fischer, and Thomas Brox. U-net: Convolutional networks for biomed-
 694 ical image segmentation, 2015. URL <https://arxiv.org/abs/1505.04597>.

695 Fatemeh Shiri, Xiao-Yu Guo, Mona Golestan Far, Xin Yu, Reza Haf, and Yuan-Fang Li. An empir-
 696 ical analysis on spatial reasoning capabilities of large multimodal models. In Yaser Al-Onaizan,
 697 Mohit Bansal, and Yun-Nung Chen (eds.), *Proceedings of the 2024 Conference on Empirical*
 698 *Methods in Natural Language Processing*, pp. 21440–21455, Miami, Florida, USA, Novem-
 699 ber 2024. Association for Computational Linguistics. doi: 10.18653/v1/2024.emnlp-main.1195.
 700 URL <https://aclanthology.org/2024.emnlp-main.1195/>.

702 Oleksii Sidorov, Ronghang Hu, Marcus Rohrbach, and Amanpreet Singh. Textcaps: a dataset for im-
 703 age captioning with reading comprehension, 2020. URL <https://arxiv.org/abs/2003.12462>.

704

705

706 Edward C Tolman. Cognitive maps in rats and men. *Psychological Review*, 55(4):189–208, 1948.

707

708 Michael Tschannen, Alexey Gritsenko, Xiao Wang, Muhammad Ferjad Naeem, Ibrahim Alabdul-
 709 mohsin, Nikhil Parthasarathy, Talfan Evans, Lucas Beyer, Ye Xia, Basil Mustafa, Olivier Hénaff,
 710 Jeremiah Harmsen, Andreas Steiner, and Xiaohua Zhai. Siglip 2: Multilingual vision-language
 711 encoders with improved semantic understanding, localization, and dense features. *arXiv preprint*
 712 *arXiv:2502.14786*, 2025. doi: 10.48550/arXiv.2502.14786.

713

714 Team Wan, Ang Wang, Baole Ai, Bin Wen, Chaojie Mao, Chen-Wei Xie, Di Chen, Feiwu Yu,
 715 Haiming Zhao, Jianxiao Yang, et al. Wan: Open and advanced large-scale video generative
 716 models. *arXiv preprint arXiv:2503.20314*, 2025.

717

718 Zhendong Wang, Yifan Jiang, Yadong Lu, Yelong Shen, Pengcheng He, Weizhu Chen, Zhangyang
 719 Wang, and Mingyuan Zhou. In-context learning unlocked for diffusion models. *arXiv preprint*
 720 *arXiv:2305.01115*, 2023. URL <https://arxiv.org/abs/2305.01115>.

721

722 Sihan Yang, Runsen Xu, Yiman Xie, Sizhe Yang, Mo Li, Jingli Lin, Chenming Zhu, Xiaochen
 723 Chen, Haodong Duan, Xiangyu Yue, Duhua Lin, Tai Wang, and Jiangmiao Pang. Mmsi-bench:
 724 A benchmark for multi-image spatial intelligence. *arXiv preprint arXiv:2505.23764*, 2025a.

725

726 Zhuoyi Yang, Jiayan Teng, Wendi Zheng, Ming Ding, Shiyu Huang, Jiazheng Xu, Yuanming Yang,
 727 Wenyi Hong, Xiaohan Zhang, Guanyu Feng, Da Yin, Yuxuan Zhang, Weihan Wang, Yean Cheng,
 728 Bin Xu, Xiaotao Gu, Yuxiao Dong, and Jie Tang. Cogvideox: Text-to-video diffusion models with
 729 an expert transformer. In *The Thirteenth International Conference on Learning Representations*,
 730 2025b. URL <https://openreview.net/forum?id=LQzN6TRFg9>.

731

732 Baiqiao Yin, Qineng Wang, Pingyue Zhang, Jianshu Zhang, Kangrui Wang, Zihan Wang, Jieyu
 733 Zhang, Keshigeyan Chandrasegaran, Han Liu, Ranjay Krishna, Saining Xie, Manling Li, Ji-
 734 ajun Wu, and Li Fei-Fei. Spatial mental modeling from limited views. *arXiv preprint*
 735 *arXiv:2506.21458*, 2025.

736

737 Xiaohua Zhai, Basil Mustafa, Alexander Kolesnikov, and Lucas Beyer. Sigmoid loss for language
 738 image pre-training, 2023. URL <https://arxiv.org/abs/2303.15343>.

739

740

741

742

743

744

745

746

747

748

749

750

751

752

753

754

755

756 **A APPENDIX**
757758 **B THE USE OF LLMS**
759760 Large language models (LLMs) were used to refine and polish writing.
761762 **C RELATED WORK**
763764 **C.1 WORLD MODELS**
765766 Various methods have been developed to learn predictive models of visual dynamics. Ha and
767 Schmidhuber (2018) proposed the original World Models framework, which learns a compressed
768 latent representation of an environment’s dynamics using generative RNNs (Ha & Schmidhuber,
769 2018). Hafner introduced PlaNet (Hafner et al., 2018) and later Dreamer (Hafner et al., 2019),
770 which use latent space dynamics models trained on pixel observations for planning and control.
771 More recently, large-scale self-supervised video models have emerged. For example, Meta’s V-JEPA
772 2 (Assran et al., 2025) and NVIDIA’s COSMOS (Agarwal et al., 2025a) provide video foundation
773 models that enable understanding, prediction, and planning from raw visual data. Zhou (2024)
774 introduced DINO-WM, a world model that leverages pretrained DINOv2 patch features to enable
775 zero-shot goal-reaching via planning in feature space (Zhou et al., 2024). Similarly, Stability AI’s
776 Stable Video Diffusion trains a high-capacity latent video diffusion model on vast video datasets for
777 high-quality text-to-video and image-to-video generation (Blattmann et al., 2023).
778779 **C.2 GENERALIST MODELS**
780781 Recent work has explored using diffusion-based generative models for flexible multi-task and in-
782 context learning. Wang (2023) presented Prompt Diffusion, a method that enables in-context learning
783 in diffusion models by conditioning on example input-output image pairs and a text prompt
784 (Wang et al., 2023). Geng (2023) proposed InstructDiffusion, a unified framework that casts di-
785 verse vision tasks as a pixel-space image manipulation guided by human instructions, learned via
786 a diffusion process (Geng et al., 2023). Bai (2024) introduced a sequential modeling approach
787 that represents images and annotations as “visual sentences,” enabling training a single large vision
788 model across many tasks without using any language data (Bai et al., 2024). Lin (2025) presented
789 RealGeneral, which reformulates image generation as conditional frame prediction analogous to
790 LLM in-context learning: using video diffusion models with novel modules, they unify multiple
791 image-generation tasks (e.g. custom generation, canny-to-image) within one framework (Lin et al.,
792 2025).
793794 **C.3 VISION ENCODERS FOR MLLMs**
795796 The choice of vision encoder is critical for multimodal LLMs. Radford (2021) introduced CLIP,
797 which learns joint image–text embeddings via contrastive pretraining on large image-caption
798 datasets (Radford et al., 2021). Building on CLIP, Tschannen (2025) developed SigLIP 2,
799 which augments the original sigmoid-contrastive objective with self-distillation, masked prediction,
800 and multilingual pretraining to improve semantic understanding, localization, and dense features
801 (Tschannen et al., 2025). Caron (2021) showed that self-supervised ViT models (DINO) learn rich
802 spatial features: their DINO model (trained with a self-distillation loss) achieves strong representa-
803 tion quality with emergent object-centric properties (Caron et al., 2021). Jiang (2023) evaluated vari-
804 ous image encoders in multimodal LLMs and proposed COMM, a simple feature-merging strategy
805 that fuses multi-layer CLIP and DINO features, demonstrating improved grounding and fine-grained
806 visual understanding in downstream tasks (Jiang et al., 2023).
807808 **D APPENDIX: MODEL FORMALIZATION**
809**VLM basics.** A frozen SigLIP image encoder E_{siglip} maps an image $x \in \mathbb{R}^{H \times W \times 3}$ to a grid of
patch embeddings $S \in \mathbb{R}^{N \times C_s}$, where N is the number of patches and C_s the channel width. A

810 lightweight projector $P_{\text{siglip}} : \mathbb{R}^{C_s} \rightarrow \mathbb{R}^d$ aligns these to the LLM token space:
 811

$$812 \quad V_s = P_{\text{siglip}}(S) = \text{MLP}_s(S) \in \mathbb{R}^{N \times d}, \quad (1)$$

813 where MLP_s is a 2-layer MLP with GELU activations.
 814

815 **SVD for single-image \rightarrow video.** Stable Video Diffusion (SVD) consists of a VAE encoder ϕ and
 816 a U-Net denoiser f_θ operating over a continuous noise scale σ (Karras et al.). Given a conditioning
 817 image x , we compute a latent $z_0 = \phi(x)$. To form a video latent tensor, we replicate z_0 across T
 818 frames:
 819

$$Z_0 = [z_0, \dots, z_0] \in \mathbb{R}^{T \times C \times H' \times W'}.$$

820 Let σ_0 denote the initial noise level from the SVD schedule. We perform one explicit Euler integra-
 821 tion step over the ODE at σ_0 (classifier-free guidance disabled):
 822

$$823 \quad Z_1 = Z_0 + \Delta\sigma f_\theta(Z_0, \sigma_0, c), \quad (2)$$

824 where c denotes SVD conditioning (e.g., time/frame embeddings, text/image prompts), and $\Delta\sigma$ is
 825 the step size.
 826

827 We do not render frames; instead, we extract a U-Net hidden activation at the lowest spatial resolu-
 828 tion on the downsampling path before the mid-block:
 829

$$H \in \mathbb{R}^{T \times H_d \times W_d \times C_h} = \text{Hidden}^{\text{pre-mid}}(f_\theta, Z_1). \quad (3)$$

830 **Multi-image extension.** For multiple images $\{x_k\}_{k=1}^K$, we first compute their latents $\{z_0^{(k)}\}$.
 831 These are inserted as keyframes within T frames at indices $i_k = \text{round}(\text{linspace}(0, T-1, K))$.
 832 We initialize Z_0 with copies of $z_0^{(1)}$ and set $(Z_0)_{i_k} \leftarrow z_0^{(k)}$ before the Euler step, yielding multi-
 833 image-aware H .
 834

835 **Static+dynamics token fusion.** We convert H into a token sequence by flattening spatial loca-
 836 tions: $L = H_d W_d$, $\tilde{H} \in \mathbb{R}^{(T \cdot L) \times C_h}$. A projector $P_{\text{svd}} : \mathbb{R}^{C_h} \rightarrow \mathbb{R}^d$ maps these to the LLM token
 837 space:
 838

$$V_d = P_{\text{svd}}(\tilde{H}) = \text{MLP}_d(\tilde{H}) \in \mathbb{R}^{M \times d}, \quad (4)$$

839 where $M = T \cdot L$.
 840

841 The SigLIP tokens \hat{V}_s (Eq. 1) are concatenated with \hat{V}_d to form the visual sequence:
 842

$$V = [\hat{V}_s; \hat{V}_d].$$

843
 844
 845
 846 **Table 4: Model Performance Across Different Frame Numbers.** These are DyVA with SVD only
 847 encoders using 5761024

Frames	Pretrain	Tuning	VQAv2	GQA	VizWiz	VSR (BL:51)	POPE	TallyQA	SeedBench	SpatialMM-Obj	3DSR-Bench-real
1	558k	665k	59.38	47.75	48.74	52.12	75.74	50.97	51.12	38.81	45.40
4	558k	665k	60.10	47.36	46.24	53.19	77.60	50.68	52.24	42.48	45.67
8	558k	665k	60.80	48.63	50.25	52.20	78.15	51.46	52.81	37.98	46.32
14	558k	665k	61.73	49.71	38.68	53.43	78.80	52.19	53.28	39.78	46.32

852
 853 **Table 5: SVD vs. SVD-MiddleBlock.** Comparison of different fusion strategies using SVD latents.

Model	VQAv2	GQA	VizWiz	VSR	POPE	TallyQA	SeedBench	Spatial	3DSR
DyVA-SVD	61.82	50.20	50.60	53.60	75.61	53.27	52.55	40.60	43.50
DyVA-SVD-Post-MiddleBlock	62.86	54.30	51.41	57.69	80.17	51.36	52.50	41.13	43.84

854
 855 **D.1 U-NET LAYER CHOICE**

856 **Passing through deeper layers in the UNet allows models to obtain better results.** Extracting
 857 latents from deeper U-Net blocks (pre-mid vs. mid) changes the balance between global layout
 858 information and fine-grained motion cues. Better latents seem to We leave exploration of the utili-
 859 zation of different latents from the world model as future work.